Plaque character and progression according to the location of coronary atherosclerotic plaque

Bax, A.M.; Yoon, Y.E.; Gianni, U.; Ma, X.Y.; Lu, Y.; Lee, B.C.; ... ; Chang, H.J.

Plaque Character and Progression According to the Location of Coronary Atherosclerotic Plaque

A. Maxim Bax, BSc[a], Yeonyee E. Yoon, MD, PhD[a,b,c,*], Umberto Gianni, MD[a], Xiaoyue Ma, MSc[d], Yao Lu, MSc[d], Benjamin C. Lee, PhD[a], Benjamin Goebel, BS[a], Donghee Han, MD[e], Sang-Eun Lee, MD, PhD[f,g], Ji Min Sung, PhD[g,h], Daniele Andreini, MD, PhD[i], Mouaz H. Al-Mallah, MD[j], Matthew J. Budoff, MD[k], Filippo Cademartiri, MD, PhD[l], Kavitha Chinnaiyan, MD[m], Jung Hyun Choi, MD, PhD[n], Eun Ju Chun, MD, PhD[c], Edoardo Conte, MD[i], Ilan Gottlieb, MD, PhD[o], Martin Hadamitzky, MD[p], Yong Jin Kim, MD, PhD[b], Byoung Kwon Lee, MD, PhD[q], Jonathon A. Leipsic, MD[r], Erica Maffei, MD[s], Hugo Marques, MD, PhD[t], Pedro de Araújo Gonçalves, MD, PhD[t,u], Gianluca Pontone, MD, PhD[i], Sanghoon Shin, MD[f], Jagat Narula, MD, PhD[x], Fay Yu-Huei Lin, MD[l], Leslee J. Shaw, PhD[l], and Hyuk-Jae Chang, MD, PhD[g,h]

Although acute coronary syndrome culprit lesions occur more frequently in the proximal coronary artery, whether the proximal clustering of high-risk plaque is reflected in earlier-stage atherosclerosis remains unclarified. We evaluated the longitudinal distribution of stable atherosclerotic lesions on coronary computed tomography angiography (CCTA) in 1,478 patients (mean age, 61 years; men, 58%) enrolled from a prospective multinational registry of consecutive patients undergoing serial CCTA. Of 3,202 coronary artery lesions identified, 2,140 left lesions were classified (based on the minimal lumen diameter location) into left main (LM, n = 128), proximal (n = 739), and other (n = 1,273), and 1,062 right lesions were classified into proximal (n = 355) and other (n = 707). Plaque volume (PV) was the highest in proximal lesions (median, 26.1 mm^3), followed by LM (20.6 mm^3) and other lesions (15.0 mm^3, p <0.001), for left lesions, and was lager in proximal (25.8 mm^3) than in other lesions (15.2 mm^3, p <0.001) for right lesions. On both sides, proximally located lesions tended to have greater necrotic core and fibrofatty components than other lesions (left: LM, 10.6%; proximal, 5.8%; other, 3.4% of the total PV, p <0.001; right: proximal, 8.4%; other 3.1%, p <0.001), with less calcified plaque component (left: LM, 18.3%; proximal, 30.3%; other, 37.7%, p <0.001; right: proximal, 23.3%, other, 36.6%, p <0.001), and tended to progress rapidly (adjusted odds ratios: left: LM, reference; proximal, 0.95, p = 0.803; other, 0.64, p = 0.017; right: proximal, reference; other, 0.52, p <0.001). Proximally located plaques were larger, with more risky composition, and progressed more rapidly. © 2021 Elsevier Inc. All rights reserved. (Am J Cardiol 2021;158:15−22)

[a]Department of Radiology, Dalio Institute of Cardiovascular Imaging, New York-Presbyterian Hospital and Weill Cornell Medicine, New York, New York; [b]Department of Internal Medicine, Seoul National University College of Medicine, Cardiovascular Center, Seoul National University Hospital, Seoul, South Korea; [c]Cardiovascular Center, Seoul National University Bundang Hospital, Sungnam, South Korea; [d]Department of Healthcare Policy and Research, New York-Presbyterian Hospital and the Weill Cornell Medical College, New York, New York; [e]Department of Imaging, Cedars-Sinai Medical Center, Los Angeles, California; [f]Division of Cardiology, Department of Internal Medicine, Ewha Womans University Seoul Hospital, Ewha Womans University College of Medicine, Seoul, South Korea; [g]Yonsei-Cedars-Sinai Integrative Cardiovascular Imaging Research Center, Yonsei University College of Medicine, Yonsei University Health System, Seoul, South Korea; [h]Division of Cardiology, Severance Cardiovascular Hospital, Yonsei University College of Medicine, Yonsei University Health System, Seoul, South Korea; [i]Centro Cardiologico Monzino, IRCCS, Milan, Italy; [j]Houston Methodist DeBakey Heart and Vascular Center, Houston Methodist Hospital, Houston, Texas; [k]Department of Medicine, Lundquist Institute at Harbor UCLA Medical Center, Torrance, California; [l]Cardiovascular Imaging Unit, SDN IRCCS, Naples, Italy; [m]Department of Cardiology, William Beaumont Hospital, Royal Oak, Michigan; [n]Department of Cardiology, Pusan University Hospital, Busan, South Korea; [o]Department of Radiology, Casa de Saude São Jose, Rio de Janeiro, Brazil; [p]Department of Radiology and Nuclear Medicine, German Heart Centre Munich, Munich, Germany; [q]Gangnam Severance Hospital, Yonsei University College of Medicine, Seoul, South Korea; [r]Department of Medicine and Radiology, University of British Columbia, Vancouver, British Columbia Canada; [s]Department of Radiology, Area Vasta 1/Azienda Sanitaria Unica Regionale (ASUR) Marche, Urbino, Italy; [t]UNICA, Unit of Cardiovascular Imaging, Hospital da Luz, Lisbon, Portugal; [u]NOVA Medical School, Lisbon, Portugal; and [x]Icahn School of Medicine at Mount Sinai, Mount Sinai Heart, Zena and Michael A. Wiener Cardiovascular Institute, and Marie-Josée and Henry R. Kravis Center for Cardiovascular Health, New York, New York. Manuscript received May 15, 2021; revised manuscript received and accepted July 16, 2021.

See page 21 for disclosure information.

*Corresponding author: Tel: (646) 962-6278; fax: (646) 962-0129.

E-mail address: yeonyeeyoon@gmail.com (Y.E. Yoon).

Although the distribution of ruptured or prone-to-rupture plaques is known to be nonuniform throughout the coronary tree,[1-4] whether the proximal clustering of high-risk plaque (HRP) is reflected in earlier stages of atherosclerosis remains unclarified. Most previous studies using invasive coronary angiography with and without intravascular ultrasound (IVUS) were innately limited to high-risk populations or patients with acute coronary syndrome, and thus, do not provide insight into the earlier stages of coronary atherosclerosis. The advent of coronary computed tomography angiography (CCTA) has enabled the noninvasive assessment of coronary atherosclerotic plaque volume (PV) and composition in lower-risk patients who are not eligible for invasive coronary angiography.[5,6] In this substudy of the Progression of Atherosclerotic Plaque Determined by Computed Tomographic Angiography Imaging (PARADIGM) study,[7] we explored the longitudinal distribution of coronary atherosclerotic plaques on CCTA, and compared the PV, composition, and progression on follow-up CCTA according to the plaque location.

Methods

The study protocol was approved by the institutional review boards of all participating centers. The study participants were recruited from the PARADIGM study, a dynamic multinational observational registry that prospectively collected clinical, procedural, and follow-up data on 2,252 consecutive patients who underwent clinically indicated serial CCTA with an inter-scan interval of ≥2 years.[7] In the current study, after excluding 492 patients with CCTA images uninterpretable for quantitative analysis and

282 patients with previous coronary revascularization before the index CCTA, 1,478 patients remained for the analysis (Figure 1).

CCTA acquisition and analysis were performed in accordance with the guidelines.[8,9] Images from each participating site were transferred to a core laboratory for blinded analysis by level III certified physicians, using semi-automated plaque analysis software (QAngioCT Research Edition v2.1.9.1, Medis Medical Imaging Systems, Leiden, the Netherlands).[10] All coronary arteries and major side branches with a diameter ≥2 mm were evaluated according to the modified 17-segment model proposed by the American Heart Association for coronary segment classification.[11] Atherosclerotic plaque was defined as any tissue ≥1 mm^2 within or adjacent to the lumen, distinguishable from surrounding structures in >2 planes. For each lesion, the distance from the ostium to the minimal lumen diameter (MLD) was measured. Coronary lesions were categorized according to the location of the MLD.[12] In the left coronary artery, lesions were classified as left main (LM), proximal (proximal left anterior descending artery or proximal left circumflex artery), or other lesions (any other segment); wherease in the right coronary artery, lesions were classified as proximal (proximal right coronary artery) or other lesions (any other segment).

For all coronary lesions, the PV (mm^3) was measured and further subclassified by composition using pre-defined Hounsfield Unit (HU) threshold cut-off values: necrotic core PV, -30 to 30 HU; fibrofatty PV, 31 to 130 HU; fibrous PV, 131 to 350 HU; and calcified PV, >350 HU.[6,8,13] To account for differences in the total vessel length between patients and to provide an equal weighting of each patient


```
┌─────────────────────────────────────────────────────────────────┐
│        2,252 patients with repeated (≥2) CCTA examination          │
└─────────────────────────────────────────────────────────────────┘
                              │
                              │      ┌──────────────────────────────────────────────────────────┐
                              ├─────▶│ • Patients with noninterpretable CCTA on 0.5 mm analysis (n=492) │
                              │      │ • Prior revascularization before baseline CCTA (n=282)          │
                              │      └──────────────────────────────────────────────────────────┘
                              ▼
┌─────────────────────────────────────────────────────────────────┐
│         1,478 patients eligible for current analysis:              │
│  3,636 lesions identified at both baseline and follow-up CCTA      │
└─────────────────────────────────────────────────────────────────┘
                              │
                              │      ┌──────────────────────────────────────────────────────────┐
                              ├─────▶│ • Separate lesions at baseline but merged into one lesion at   │
                              │      │   follow-up (n=190)                                            │
                              │      │ • Revascularized lesions after baseline CCTA (n=244)           │
                              │      └──────────────────────────────────────────────────────────┘
                              ▼
┌─────────────────────────────────────────────────────────────────┐
│     3,202 lesions with both baseline and follow-up CCTA analysis   │
└─────────────────────────────────────────────────────────────────┘
                   │                                 │
                   ▼                                 ▼
     ┌──────────────────────────┐       ┌──────────────────────────┐
     │ 2,140 left coronary lesions │       │ 1,062 right coronary lesions │
     └──────────────────────────┘       └──────────────────────────┘
                   │                                 │
                   ▼                                 ▼
     ┌──────────────────────────┐       ┌──────────────────────────┐
     │ • 128 left main lesions   │       │ • 355 proximal lesions    │
     │ • 739 proximal lesions    │       │ • 707 other lesions       │
     │ • 1,273 other lesions     │       │                           │
     └──────────────────────────┘       └──────────────────────────┘
```
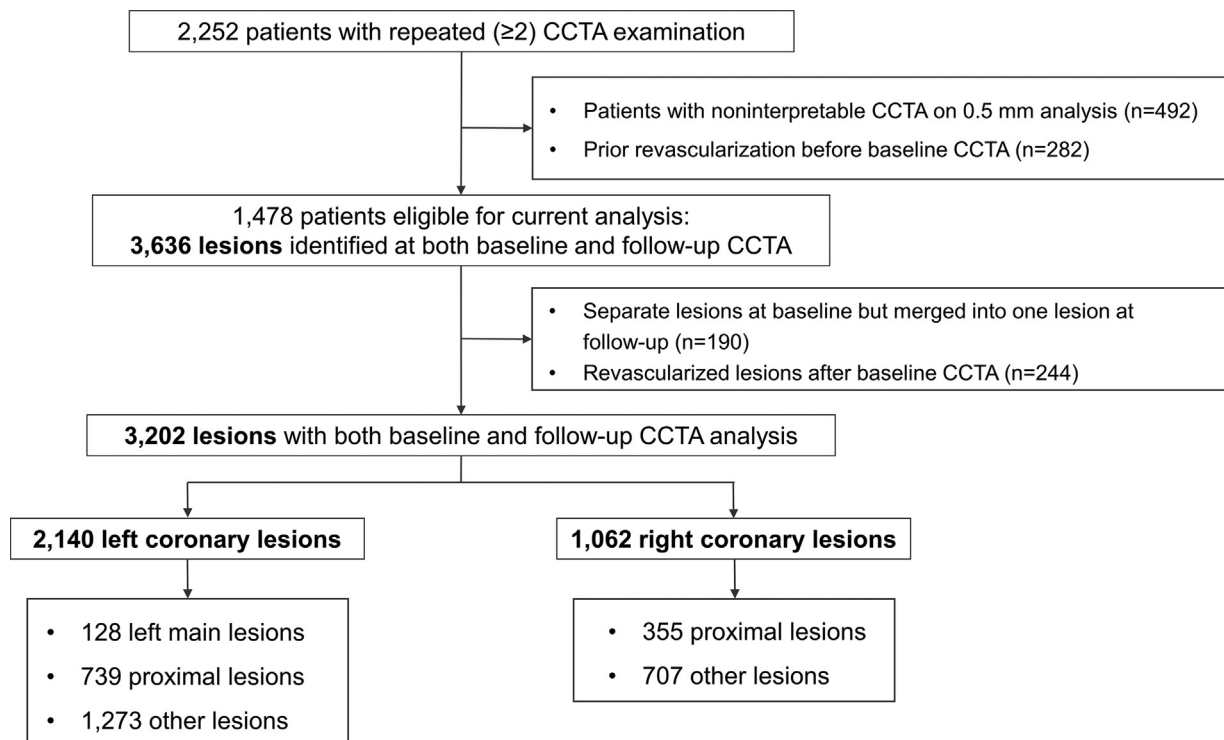
Figure 1. Study flow
CCTA = coronary computed tomographic angiography.

in the calculation of PV, we normalized the PV as ([absolute PV/total vessel length] * mean population vessel length).[14]

To explore the compositional differences according to longitudinal lesion location, the compositional makeup of each lesion was evaluated by calculating the volume percent (%vol) of each component as (component PV/total PV * 100, %). Additionally, lesions were classified as noncalcified (no calcium), mixed ($\leq$70% volume calcified plaque), or calcified (>70% volume calcified plaque), based on a visual estimation.[13] Furthermore, coronary lesions were classified as HRP if $\geq$2 previously defined HRP features linked to plaque rupture and subsequent adverse outcomes (spotty calcification, positive remodeling, and low-attenuation plaque) were present.[15,16] Diameter and area stenosis were quantified as the percent of the reduction in lumen diameter and area.

To evaluate the progression or regression of each lesion, lesions were matched between the index and follow-up CCTA using fiduciary landmarks, such as coronary side branches. Annualized changes in total and compositional PV were calculated as (ΔPV/CCTA interval, mm^3/year). The median value of the annual total PV change for each location of left and right coronary lesions was used to define rapid plaque progression.[17,18]

All analyses were performed in SPSS (version 25; IBM Corp., Armonk, NY) and R Studio (version 3.6.3). Continuous variables are presented as median (interquartile range [IQR]), and categorical variables are presented as numbers (percentages). Continuous variables were compared using the independent t-test, Mann-Whitney U test, analysis of variance, or Kruskal-Wallis test, as appropriate. Categorical variables were compared using the Chi-square or Fisher's exact test. Multiple comparison adjustment was performed using Bonferroni's correction or Dunn's post-hoc testing, as appropriate. To compare the risk for rapid plaque progression according to lesion location whereas accounting for within-patient clustering of lesion data, logistic generalized estimating equation (GEE) models were used, with adjustment for common within-patient factors (10-year atherosclerotic cardiovascular disease [ASCVD] risk, statin use at follow-up) and baseline PV. Results are presented as adjusted odds ratios (aORs) with corresponding 95% confidence intervals (CIs). Two-tailed p-values <0.05 were considered statistically significant.

Results

In total, 1,478 patients (median 61 [54 to 67] years, men 58.4%) were included and their clinical characteristics are shown in Table 1. The median interscan interval between baseline and follow-up CCTA was 3.3 (2.6 to 4.8) years. Overall, 3,202 coronary artery lesions analyzed on both baseline and follow-up CCTA were identified (median diameter stenosis 16 [9 to 26]%, area stenosis 30 [16 to 45]%); 2,140 were left coronary lesions and 1,062 were right coronary artery lesions (Figure 1). In the longitudinal distributions of the coronary lesions, left coronary lesions showed a positively skewed unimodal distribution, with a median distance from the ostium to the MLD of 31.9 (20.6 to 44.8) mm, whereas right coronary lesions showed a

Table 1
Clinical characteristics and lipid profiles

Variable	Study population (n = 1,478)
Age (years)	61 [54; 67]
Men	863 (58.4%)
Body mass index (kg/m^2)	25.0 [23.2; 27.2]
10-year ASCVD risk (%)	9.8 [4.9; 18.7]
Low to borderline (<7.5%)	583 (39.4%)
Intermediate (7.5-20%)	567 (38.4%)
High (>20%)	328 (22.2%)
Hypertension	790 (53.8%)
Diabetes mellitus	303 (20.6%)
Hyperlipidemia	575 (39.2%)
Smoking	263 (17.9%)
Family history of CAD	432 (29.2%)
Symptoms	
Typical chest pain	71 (4.8%)
Atypical chest pain	1020 (69.5%)
Noncardiac chest pain	136 (9.3%)
Shortness of breath	120 (8.2%)
Asymptomatic	224 (15.3%)
Medications at baseline	
Aspirin	558 (37.8%)
RAAS inhibitor	420 (28.4%)
Statins	590 (39.9%)
Lipid profile at baseline (mg/dL)	
Total cholesterol	189.0 [163.0; 215.0]
Triglycerides	123.0 [89.0; 178.0]
High-density lipoprotein	49.0 [41.0; 58.0]
Low-density lipoprotein	115.0 [91.0; 138.0]
Medications at follow-up	
Statins	811 (54.9%)
Lipid profile at follow-up (mg/dL)	
Total cholesterol	169.0 [145.0; 198.0]
Triglycerides	111.0 [79.0; 158.8]
High-density lipoprotein	48.0 [41.0; 57.0]
Low-density lipoprotein	96.9 [77.0; 123.0]

Data are presented as the median (interquartile range) for continuous variables and number (percentage) for categorical variables. Patients could present with >1 symptom.

ASCVD = atherosclerotic cardiovascular disease, CAD = coronary artery disease, RAAS = renin-angiotensin-aldosterone system.

bimodal distribution, with a median distance from the ostium to the MLD of 50.0 [25.0 to 97.9] mm (Figure 2).

In the comparisons of baseline CCTA characteristics of left coronary artery lesions according to location (LM 6.0%, proximal 34.5%, and other lesions 59.5%), the total PV of proximal lesions (median 26.1 mm^3) was comparable to that of LM lesions (20.6 mm^3; p = 0.178), but was significantly greater than that in other lesions (15.0 mm^3; p <0.001) (Table 2). In the right coronary artery (proximal 33.4%, and other lesions 66.6%), the total PV was greater in proximal lesions (25.8 mm^3) than in other lesions (15.2 mm^3; p <0.001). In the evaluation of the stenosis severity in left coronary artery lesions, the diameter stenosis gradually increased from LM lesions to proximal and other lesions (p <0.001). However, for right coronary artery lesions, the diameter stenosis did not significantly differ between proximal and other lesions (p = 0.068).

Plaque composition also changed according to the longitudinal lesion location. More proximally located lesions tended to have greater necrotic core and fibrofatty PVs
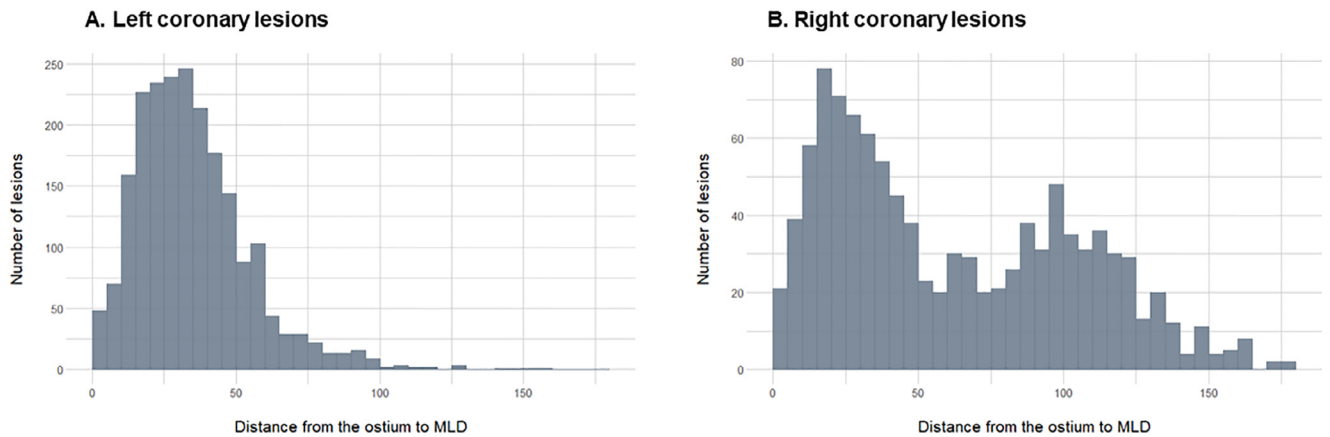
Longitudinal Distribution of Coronary Lesions

Figure 2. Longitudinal distribution of left and right coronary lesions. In the histograms, the number of lesions is indicated according to the distance from the ostium to the MLD of the lesion. MLD = minimal lumen diameter.

compared with those in distally located lesions (Figure 3). Concordantly, LM lesions showed the highest necrotic core and fibrofatty plaque %vol, followed by proximal and other lesions (median 10.6%, 5.8%, and 3.4%, respectively; p <0.001) (Table 2). On the other hand, the calcified plaque %vol was the lowest in LM lesions and gradually increased from proximal to other lesions (18.3%, 30.3%, and 37.7%, respectively; p <0.001). Similarly, in the right coronary artery, the necrotic core and fibrofatty plaque %vol was greater in proximal lesions than in other lesions (8.4% and 3.1%, respectively; p <0.001), whereas the calcified plaque %vol was lower in proximal lesions than in other

lesions (23.3% and 36.6%, respectively; p <0.001). In both left and right coronary arteries, the distance from the ostium to the MLD was inversely related to the necrotic core and fibrofatty plaque %vol and positively related to the calcified plaque %vol (Supplemental Figure 1).

Visual compositional classification of the coronary lesions showed similar results. Among left coronary artery lesions, LM lesions showed the highest prevalence of non-calcified lesions, whereas proximal lesions showed the highest prevalence of mixed lesions, and other lesions showed the highest prevalence of calcified lesions (p <0.001). Similarly, among right coronary artery lesions,

Table 2
Baseline CCTA characteristics according to longitudinal distribution

Variable	Left coronary lesions (n = 2,140)				Right coronary lesions (n = 1,062)		
	Left main (n = 128)	Proximal (n = 739)	Others (n = 1,273)	p	Proximal (n = 355)	Others (n = 707)	p
Lesion length (mm)	14.1 [10.8;17.6][†,‡]	18.7 [13.7;27.2]*,‡	16.8 [13.0;27.6]*,†	<0.001	17.9 [14.4;26.9]	15.8 [12.9;24.3]	<0.001
Normalized PV (mm³)	20.6 [11.5;38.4]	26.1 [10.0;71.1]‡	15.0 [6.1;48.0]†	<0.001	25.8 [11.8;63.3]	15.2 [6.8;41.8]	<0.001
%vol of each component							
Necrotic core	0.0 [0.0; 2.0]‡	0.0 [0.0; 0.6]‡	0.0 [0.0; 0.2]*,†	<0.001	0.0 [0.0; 1.0]	0.0 [0.0; 0.2]	<0.001
Fibrofatty plaque	9.8 [1.2;31.8][†,‡]	5.7 [0.5;23.8]*,‡	3.3 [0.0;16.8]*,†	<0.001	7.9 [0.8;30.2]	3.1 [0.0;14.5]	<0.001
Necrotic core + Fibrofatty plaque	10.6 [1.2;37.2]	5.8 [0.5; 25.4]	3.4 [0.0; 17.4]	<0.001	8.4 [0.8; 31.8]	3.1 [0.0; 15.0]	<0.001
Fibrous plaque	50.5 [37.9;64.4]	48.7 [32.8;64.8]	47.5 [30.6;62.5]	0.064	54.8 [37.9;67.2]	50.2 [32.6;65.9]	0.017
Calcified plaque	18.3 [2.4;47.1][†,‡]	30.3 [4.9;59.4]*,‡	37.7 [11.8;64.3]*,†	<0.001	23.3 [2.2;50.4]	36.6 [11.5;61.2]	<0.001
Plaque composition							
Noncalcified	32 (25.0%)[†,‡]	154 (20.8%)*,‡	188 (14.8%)*,†	<0.001	101 (28.5%)	118 (16.7%)	<0.001
Mixed	41 (32.0%)	301 (40.7%)	451 (35.4%)		120 (33.8%)	213 (30.1%)	
Calcified	55 (43.0%)	284 (38.4%)	634 (49.8%)		134 (37.7%)	376 (53.2%)	
HRP lesions	25 (19.5%)	134 (18.1%)‡	175 (13.7%)†	0.015	69 (19.4%)	103 (14.6%)	0.052
Diameter stenosis	11.2 [5.7;19.1][†,‡]	16.0 [8.0;25.8]*,‡	18.0 [9.9;28.2]*,†	<0.001	15.5 [8.4;25.6]	14.0 [7.5;22.7]	0.068
Area stenosis (%)	21.0 [11.3;34.6][†,‡]	29.4 [15.3;44.9]*,‡	32.7 [18.9;48.5]*,†	<0.001	28.6 [16.0;44.6]	26.1 [14.4;40.2.7]	0.069

Data are presented as the median (interquartile range) for continuous variables and number (percentage) for categorical variables. CCTA = coronary computed tomography angiography, HRP = high risk plaque (≥2 of: spotty calcification, low-attenuation plaque or positive remodelling), PV = plaque volume.
* Adjusted *P*-value for comparison with left main lesions <0.05.
† Adjusted *P*-value for comparison with left proximal lesions <0.05.
‡ Adjusted *P*-value for comparison with left other lesions.

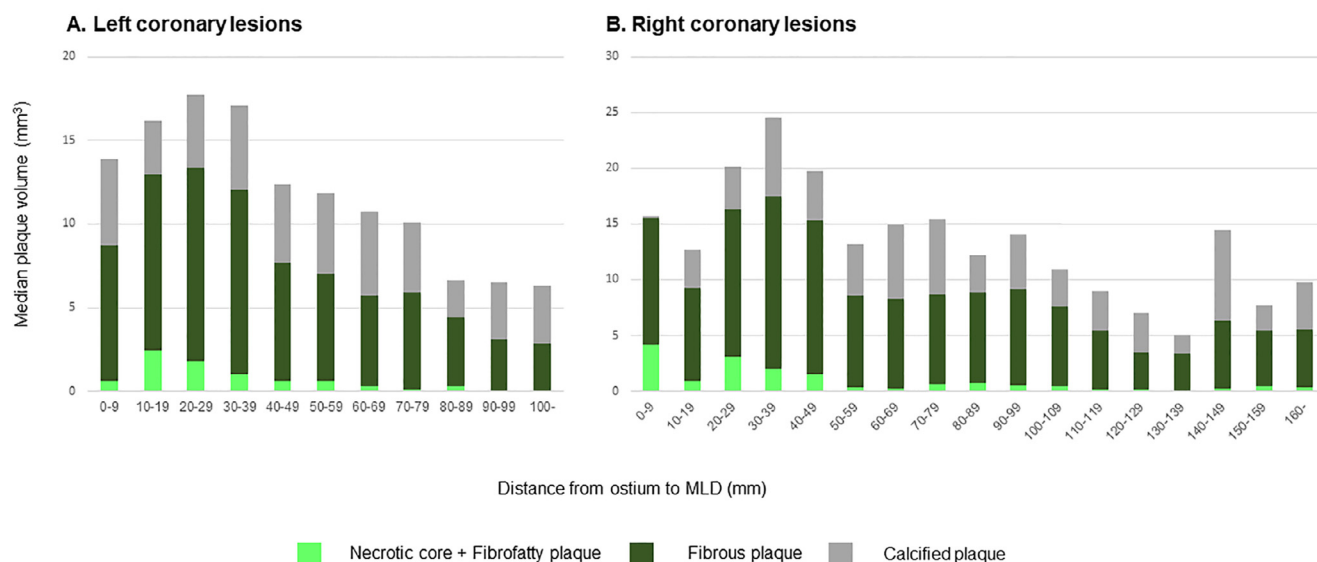## Baseline Median Plaque Volume of Each Component

Figure 3. Baseline median plaque volume of each component. The median volume of each component is presented according to the distance from the ostium to the MLD of the lesion. Proximal lesions were larger and showed greater necrotic core and fibrofatty component volumes. MLD = minimal lumen diameter.

noncalcified lesions were more prevalent in proximal lesions, whereas calcified plaques were more prevalent among other lesions (p <0.001). Among the left coronary artery lesions, the prevalence of HRP in proximal lesions (18.1%) was comparable to that for LM lesions (19.5%; p = 1.000) and significantly higher than that in other lesions (13.7%; p = 0.031). Among the right coronary artery lesions, although HRP was more commonly observed in proximal lesions than in other lesions (19.4% and 14.6%, respectively), statistical significance was not reached (p = 0.052).

Among left coronary artery lesions, the annual progression in total PV of proximal lesions (median 2.4 mm^3/year) was comparable to that in LM lesions (2.4 mm^3/year; p = 0.444), but significantly higher than that in other lesions (1.5 mm^3/year; p = 0.001) (Table 3). Notably, the proportion of all PV progression attributable to calcified plaque

gradually increased from LM lesions to proximal and other lesions (38%, 75%, and 80%, respectively). Among right coronary artery lesions, the annual progression in total PV was significantly higher in proximal lesions (3.6 mm^3/year) than in other lesions (1.7 mm^3/year; p <0.001). The proportion of all PV progression attributable to calcified plaque was higher among other lesions (82%) than in proximal lesions (50%). Distally located lesions showed a lower annual progression in their total PV than more proximally located lesions, and their progression was mainly attributable to calcified plaque (Figure 4).

In the adjusted logistic GEE models for left coronary artery lesions, the risk for rapid plaque progression was similar for LM and proximal lesions (aOR = 0.95; p = 0.803) (Table 4). However, the risk for rapid progression was significantly lower in other lesions than in LM lesions (aOR = 0.64; p = 0.017). Additionally, per 10-mm

Table 3
Annualized progression of lesions according to longitudinal distribution

	Left coronary lesions (n = 2,140)				Right coronary lesions (n = 1,062)		
	Left main (n = 128)	Proximal (n = 739)	Others (n = 1,273)	p	Proximal (n = 355)	Others (n = 707)	p
Annualized progression (mm^3/year)							
Total plaque volume	2.4 [0.2; 6.3]	2.4 [0.4; 6.9][‡]	1.5 [0.2; 5.1][†]	0.002	3.6 [0.7; 9.2]	1.7 [0.2; 5.2]	0.000
Necrotic core	0.0 [-0.0; 0.0]	0.0 [-0.0; 0.0]	0.0 [0.0; 0.0]	0.366	0.0 [-0.0; 0.0]	0.0 [0.0; 0.0]	0.910
Fibrofatty plaque	0.0 [-0.2; 0.5]	0.0 [-0.5; 0.2]	0.0 [-0.2; 0.1]	0.316	0.0 [-0.8; 0.4]	0.0 [-0.2; 0.1]	0.558
Necrotic core + Fibrofatty plaque	0.0 [-0.3; 0.5]	0.0 [-0.6; 0.3]	0.0 [-0.3; 0.1]	0.538	0.0 [-0.8; 0.4]	0.0 [-0.2; 0.1]	0.491
Fibrous plaque	0.7 [-0.3; 3.7][‡]	0.4 [-0.8; 2.7][‡]	0.1 [-0.5; 1.6]*,[†]	0.003	0.8 [-0.5; 4.0]	0.1 [-0.7; 1.7]	0.000
Calcified plaque	0.9 [0.1; 2.9][†,‡]	1.8 [0.5; 4.8]*,[‡]	1.2 [0.3; 3.6]*,[†]	0.000	1.8 [0.5; 5.5]	1.4 [0.4; 3.8]	0.011

Data are presented as the median (interquartile range) for continuous variables and number (percentage) for categorical variables.

* Adjusted *P*-values for comparisons with left main lesions <0.05.

[†] Adjusted *P*-values for comparisons with left proximal lesions <0.05.

[‡] Adjusted *P*-values for comparisons with left other lesions <0.05.
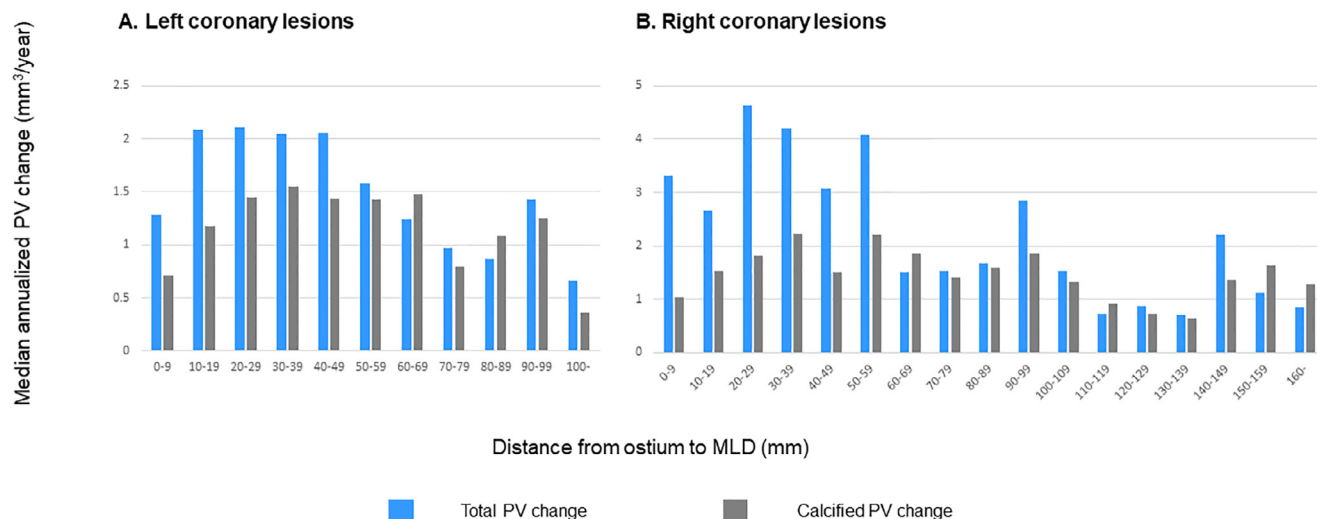
Annual Plaque Volume Progression

Figure 4. The median annualized plaque volume change. The median annualized changes in total (blue) and calcified (gray) plaque volumes are presented according to the distance from the ostium to the MLD of the lesion. In both coronary arteries (left and right), proximal lesions showed greater total plaque volume increase, with less contribution from the calcified plaque component. MLD = minimal lumen diameter.

increase in distance from the ostium to the MLD, the risk for rapid plaque progression decreased by 7% (aOR = 0.93; p = 0.001). Among right coronary artery lesions, the risk for rapid plaque progression was lower for other lesions than for proximal lesions (aOR = 0.52; p <0.001). Per 10-mm increase in distance from the ostium to the MLD, the risk for rapid progression decreased by 9% (aOR = 0.91; p <0.001). A representative case is shown in the Graphical Abstract.

Table 4
Adjusted odds ratios for rapid progression in left and right coronary artery lesions

	aOR (95% CI)*	p Value
Left coronary lesions		
Location of MLD		
Left main lesions	*ref.*	.
Proximal lesions	0.95 (0.65-1.40)	0.803
Other lesions	0.64 (0.44-0.92)	0.017
Distance from ostium to MLD		
Per 10-mm increase	0.93 (0.87-0.97)	0.001
Right coronary lesions		
Location of MLD		
Proximal lesions	*ref.*	.
Other lesions	0.52 (0.40-0.67)	<0.001
Distance from ostium to MLD		
Per 10-mm increase	0.91 (0.88-0.94)	<0.001

  * aORs for rapid plaque progression, as calculated from a logistic GEE model, with covariate adjustment for 10-year ASCVD risk, total plaque volume, and statin use at the time of follow-up CCTA.

  aOR = adjusted odds ratio, ASCVD = atherosclerotic cardiovascular disease, CCTA = coronary computed tomography angiography, CI = confidence interval, GEE = generalized estimating equation, MLD = minimal lumen diameter.

Discussion

The current analysis of coronary lesions from the PARADIGM registry revealed a difference in the longitudinal distribution of lesions in the left versus right coronary artery. Despite the difference, proximally located lesions were larger and had greater necrotic core and fibrofatty plaque components, whereas distally located lesions were smaller and had a greater calcified plaque component, in both left and right coronary arteries. Furthermore, proximally located lesions were at higher risk for rapid plaque progression, even after adjustment for 10-year ASCVD risk, statin use, and baseline PV.

Early angiographic studies have highlighted the proximal location in the coronary arteries as a clustering site of culprit lesions in acute coronary syndrome.[2,3] Gibson et al analyzed 1,914 patients with ST-elevation acute myocardial infarction (STEMI) and found that 75% of all culprit lesions were located within 60 mm of the coronary ostium.[2] Wang et al evaluated 496 patients with STEMI and found that the risk of a coronary occlusion decreased significantly per 10-mm increase in distance from the ostium in all coronary arteries.[3] In the current study, which examined a relatively lower-risk population of patients undergoing serial CCTA, we also noted a proximal clustering of coronary lesions. The proximal clustering of coronary plaques from an earlier stage of atherosclerosis could potentially reflect the future site of culprit lesions.

The current study elaborates on previous invasive study findings by portraying the differences between proximal and distal lesions in earlier stages of atherosclerosis. In a substudy of the Providing Regional Observations to Study Predictors of Events in the Coronary Tree (PROSPECT) study, which performed 3-vessel grayscale IVUS on patients presenting with acute coronary syndrome, the

highest plaque burden was observed in the most proximal 30-mm segment of each coronary artery.[12] In the current study, proximally located lesions were significantly larger than distal lesions at baseline. The clinical relevance of these findings is underscored by further evidence from the PROSPECT study, which reported an independent association between both lesion location and size, and the risk for future plaque rupture.[19] Importantly, we firstly found a significantly higher risk for rapid plaque progression in proximal lesions than in distally located lesions. Considering that plaque progression as measured on invasive and noninvasive imaging modalities is known as independently related to future adverse cardiovascular events,[20,21] clinicians should be aware of the risk for rapid plaque progression in proximal lesions, even when their diameter stenosis is not as severe as distal lesions.

In this study, in addition to a higher plaque burden, proximally located lesions tended have more high-risk characteristics related to plaque rupture and adverse cardiac outcomes than distal lesions. The Incident COroNary Syndromes Identified by Computed Tomography (ICONIC) study previously reported that necrotic core and fibrofatty PVs, as well as HRP, increased the risk for acute coronary syndrome, independent of diameter stenosis, and total plaque burden.[22] We analyzed the plaque composition in a similar fashion and found that proximally located lesions had greater necrotic core and fibrofatty plaque components. Furthermore, HRP, linked to plaque rupture and subsequent adverse cardiac events,[15,16,23] was more commonly observed in proximal lesions than in distal lesions. Therefore, our study results suggest that proximally located lesions have a higher risk for plaque rupture, as well as plaque progression, from an earlier stage of atherosclerosis.

A higher coronary artery calcium score is a well-known indicator of increased risk for future adverse cardiovascular events.[24,25] However, recent studies have demonstrated that calcified plaque is a risk marker for cardiovascular events because of its strong association with the total PV.[26,27] When considered as a percentage of the total PV, increased calcified plaque component is associated with plaque stability and reduced risk.[26] Interestingly, in the present study, not only did proximal lesions have more high-risk characteristics, they also showed lower calcified plaque %vol. Furthermore, a lesser part of plaque progression was attributable to calcified plaque in proximal lesions. The combination of these findings potentially reflects a more common plaque composition profile related to higher risk for future rupture among proximally located lesions than among more distally located lesions.

The current study has several limitations. First, the PARADIGM study enrolled patients with repeated CCTA scanning. Since patients with more rapid plaque progression were more likely to experience clinical events and might not undergo a second CCTA, the study population tended to represent patients with coronary artery disease at lower risk. Furthermore, large, proximal lesions were most likely underrepresented, since those lesions were likely to be revascularized after a first CCTA, and thus were excluded from the study analysis. Nonetheless, in this study, proximally located lesions were significantly larger and had more risk features than distal lesions. These results emphasize marked differences between proximal and distal lesions. Secondly, the current lesion classification according to the location of the MLD[12] did not account for lesion extent. In long lesions, the location of the MLD may not always reflect where the majority of the lesion is located. Thirdly, as occurs in all CCTA studies, bias due to partial-volume artifacts was inevitable.[28]

In conclusion, proximally located plaques were larger at baseline, with a composition associated with a higher risk for future plaque rupture, and progressed more rapidly than distally located plaques. These differences were found in a lower-risk population, and thus potentially impact the active preventive strategy for those with proximal coronary atherosclerotic lesions at an earlier stage, without significant luminal narrowing.

Disclosures

Acknowledgment

Supplementary materials

Supplementary material associated with this article can be found in the online version at https://doi.org/10.1016/j.amjcard.2021.07.040.

1. Kolodgie FD, Burke AP, Farb A, Gold HK, Yuan J, Narula J, Finn AV, Virmani R. The thin-cap fibroatheroma: a type of vulnerable plaque: the major precursor lesion to acute coronary syndromes. *Curr Opin Cardiol* 2001;16:285–292.
2. Gibson CM, Kirtane AJ, Murphy SA, Karha J, Cannon CP, Giugliano RP, Roe MT, Harrington RA, Ohman EM, Antman EM. Distance from the coronary ostium to the culprit lesion in acute ST-elevation myocardial infarction and its implications regarding the potential prevention of proximal plaque rupture. *J Thromb Thrombolysis* 2003;15:189–196.
3. Wang JC, Normand SL, Mauri L, Kuntz RE. Coronary artery spatial distribution of acute myocardial infarction occlusions. *Circulation* 2004;110:278–284.
4. Hong MK, Mintz GS, Lee CW, Lee BK, Yang TH, Kim YH, Song JM, Han KH, Kang DH, Cheong SS, Song JK, Kim JJ, Park SW, Park SJ. The site of plaque rupture in native coronary arteries: a three-vessel intravascular ultrasound analysis. *J Am Coll Cardiol* 2005;46:261–265.
5. Boogers MJ, Broersen A, van Velzen JE, de Graaf FR, El-Naggar HM, Kitslaar PH, Dijkstra J, Delgado V, Boersma E, de Roos A, Schuijf JD, Schalij MJ, Reiber JH, Bax JJ, Jukema JW. Automated quantification of coronary plaque with computed tomography: comparison with intravascular ultrasound using a dedicated registration algorithm for fusion-based quantification. *Eur Heart J* 2012;33:1007–1016.
6. de Graaf MA, El-Naggar HM, Boogers MJ, Veltman CE, Broersen A, Kitslaar PH, Dijkstra J, Kroft LJ, Al Younis I, Reiber JH, Bax JJ, Delgado V, Scholte AJ. Automated quantitative coronary computed tomography correlates of myocardial ischaemia on gated myocardial perfusion SPECT. *Eur J Nucl Med Mol Imaging* 2013;40:1171–1180.

7. Lee SE, Chang HJ, Rizvi A, Hadamitzky M, Kim YJ, Conte E, Andreini D, Pontone G, Volpato V, Budoff MJ, Gottlieb I, Lee BK, Chun EJ, Cademartiri F, Maffei E, Marques H, Leipsic JA, Shin S, Choi JH, Chung N, Min JK. Rationale and design of the Progression of AtheRosclerotic PlAque DetermIned by Computed TomoGraphic Angiography IMaging (PARADIGM) registry: a comprehensive exploration of plaque progression and its impact on clinical outcomes from a multicenter serial coronary computed tomographic angiography study. *Am Heart J* 2016;182:72–79.

8. Lee SE, Chang HJ, Sung JM, Park HB, Heo R, Rizvi A, Lin FY, Kumar A, Hadamitzky M, Kim YJ, Conte E, Andreini D, Pontone G, Budoff MJ, Gottlieb I, Lee BK, Chun EJ, Cademartiri F, Maffei E, Marques H, Leipsic JA, Shin S, Choi JH, Chinnaiyan K, Raff G, Virmani R, Samady H, Stone PH, Berman DS, Narula J, Shaw LJ, Bax JJ, Min JK. Effects of statins on coronary atherosclerotic plaques: the PARADIGM Study. *JACC Cardiovasc Imaging* 2018;11:1475–1484.

9. Abbara S, Blanke P, Maroules CD, Cheezum M, Choi AD, Han BK, Marwan M, Naoum C, Norgaard BL, Rubinshtein R, Schoenhagen P, Villines T, Leipsic J. SCCT guidelines for the performance and acquisition of coronary computed tomographic angiography: a report of the Society of Cardiovascular Computed Tomography Guidelines Committee: endorsed by the North American Society for Cardiovascular Imaging (NASCI). *J Cardiovasc Comput Tomogr* 2016;10:435–449.

10. Park HB, Lee BK, Shin S, Heo R, Arsanjani R, Kitslaar PH, Broersen A, Dijkstra J, Ahn SG, Min JK, Chang HJ, Hong MK, Jang Y, Chung N. Clinical feasibility of 3D automated coronary atherosclerotic plaque quantification algorithm on coronary computed tomography angiography: comparison with intravascular ultrasound. *Eur Radiol* 2015;25:3073–3083.

11. Leipsic J, Abbara S, Achenbach S, Cury R, Earls JP, Mancini GJ, Nieman K, Pontone G, Raff GL. SCCT guidelines for the interpretation and reporting of coronary CT angiography: a report of the Society of Cardiovascular Computed Tomography Guidelines Committee. *J Cardiovasc Comput Tomogr* 2014;8:342–358.

12. Wykrzykowska JJ, Mintz GS, Garcia-Garcia HM, Maehara A, Fahy M, Xu K, Inguez A, Fajadet J, Lansky A, Templin B, Zhang Z, de Bruyne B, Weisz G, Serruys PW, Stone GW. Longitudinal distribution of plaque burden and necrotic core-rich plaques in nonculprit lesions of patients presenting with acute coronary syndromes. *JACC Cardiovasc Imaging* 2012;5:S10–S18.

13. Achenbach S, Moselewski F, Ropers D, Ferencik M, Hoffmann U, MacNeill B, Pohle K, Baum U, Anders K, Jang IK, Daniel WG, Brady TJ. Detection of calcified and noncalcified coronary atherosclerotic plaque by contrast-enhanced, submillimeter multidetector spiral computed tomography: a segment-based comparison with intravascular ultrasound. *Circulation* 2004;109:14–17.

14. van Rosendael AR, Lin FY, Ma X, van den Hoogen IJ, Gianni U, Al Hussein O, Al'Aref SJ, Peña JM, Andreini D, Al-Mallah MH, Budoff MJ, Cademartiri F, Chinnaiyan K, Choi JH, Conte E, Marques H, de Araújo Gonçalves P, Gottlieb I, Hadamitzky M, Leipsic JA, Maffei E, Pontone G, Raff GL, Shin S, Kim YJ, Lee BK, Chun EJ, Sung JM, Lee SE, Berman DS, Virmani R, Samady H, Stone PH, Narula J, Bax JJ, Shaw LJ, Min JK, Chang HJ. Percent atheroma volume: optimal variable to report whole-heart atherosclerotic plaque burden with coronary CTA, the PARADIGM study. *J Cardiovasc Comput Tomogr* 2020;14:400–406.

15. Motoyama S, Ito H, Sarai M, Kondo T, Kawai H, Nagahara Y, Harigaya H, Kan S, Anno H, Takahashi H, Naruse H, Ishii J, Hecht H, Shaw LJ, Ozaki Y, Narula J. Plaque characterization by coronary computed tomography angiography and the likelihood of acute coronary events in mid-term follow-up. *J Am Coll Cardiol* 2015;66:337–346.

16. Puchner SB, Liu T, Mayrhofer T, Truong QA, Lee H, Fleg JL, Nagurney JT, Udelson JE, Hoffmann U, Ferencik M. High-risk plaque detected on coronary CT angiography predicts acute coronary syndromes independent of significant stenosis in acute chest pain: results from the ROMICAT-II trial. *J Am Coll Cardiol* 2014;64:684–692.

17. Han D, Kolli KK, Al'Aref SJ, Baskaran L, van Rosendael AR, Gransar H, Andreini D, Budoff MJ, Cademartiri F, Chinnaiyan K, Choi JH, Conte E, Marques H, de Araujo Goncalves P, Gottlieb I, Hadamitzky M, Leipsic JA, Maffei E, Pontone G, Raff GL, Shin S, Kim YJ, Lee BK, Chun EJ, Sung JM, Lee SE, Virmani R, Samady H, Stone P, Narula J, Berman DS, Bax JJ, Shaw LJ, Lin FY, Min JK, Chang HJ. Machine learning framework to identify individuals at risk of rapid progression of coronary atherosclerosis: from the PARADIGM Registry. *J Am Heart Assoc* 2020;9:e013958.

18. Lee SE, Sung JM, Rizvi A, Lin FY, Kumar A, Hadamitzky M, Kim YJ, Conte E, Andreini D, Pontone G, Budoff MJ, Gottlieb I, Lee BK, Chun EJ, Cademartiri F, Maffei E, Marques H, Leipsic JA, Shin S, Hyun Choi J, Chinnaiyan K, Raff G, Virmani R, Samady H, Stone PH, Berman DS, Narula J, Shaw LJ, Bax JJ, Min JK, Chang HJ. Quantification of coronary atherosclerosis in the assessment of coronary artery disease. *Circ Cardiovasc Imaging* 2018;11:e007562.

19. Zheng B, Mintz GS, McPherson JA, De Bruyne B, Farhat NZ, Marso SP, Serruys PW, Stone GW, Maehara A. Predictors of plaque rupture within nonculprit fibroatheromas in patients with acute coronary syndromes: the PROSPECT study. *JACC Cardiovasc Imaging* 2015;8:1180–1187.

20. Nicholls SJ, Hsu A, Wolski K, Hu B, Bayturan O, Lavoie A, Uno K, Tuzcu EM, Nissen SE. Intravascular ultrasound-derived measures of coronary atherosclerotic plaque burden and clinical outcome. *J Am Coll Cardiol* 2010;55:2399–2407.

21. van Rosendael AR, Lin FY, van den Hoogen IJ, Ma X, Gianni U, Al Hussein Alawamlh O, Al'Aref SJ, Pena JM, Andreini D, Budoff MJ, Cademartiri F, Chinnaiyan K, Choi JH, Conte E, Marques H, de Araujo Goncalves P, Gottlieb I, Hadamitzky M, Leipsic J, Maffei E, Pontone G, Raff GL, Shin S, Kim YJ, Lee BK, Chun EJ, Sung JM, Lee SE, Han D, Berman DS, Virmani R, Samady H, Stone P, Narula J, Bax JJ, Shaw LJ, Min JK, Chang HJ. Progression of whole-heart atherosclerosis by coronary CT and major adverse cardiovascular events. *J Cardiovasc Comput Tomogr* 2021;15(4):322–330.

22. Chang HJ, Lin FY, Lee SE, Andreini D, Bax J, Cademartiri F, Chinnaiyan K, Chow BJW, Conte E, Cury RC, Feuchtner G, Hadamitzky M, Kim YJ, Leipsic J, Maffei E, Marques H, Plank F, Pontone G, Raff GL, van Rosendael AR, Villines TC, Weirich HG, Al'Aref SJ, Baskaran L, Cho I, Danad I, Han D, Heo R, Lee JH, Rivzi A, Stuijfzand WJ, Gransar H, Lu Y, Sung JM, Park HB, Berman DS, Budoff MJ, Samady H, Shaw LJ, Stone PH, Virmani R, Narula J, Min JK. Coronary atherosclerotic precursors of acute coronary syndromes. *J Am Coll Cardiol* 2018;71:2511–2522.

23. Nakazato R, Otake H, Konishi A, Iwasaki M, Koo BK, Fukuya H, Shinke T, Hirata K, Leipsic J, Berman DS, Min JK. Atherosclerotic plaque characterization by CT angiography for identification of high-risk coronary artery lesions: a comparison to optical coherence tomography. *Eur Heart J Cardiovasc Imaging* 2015;16:373–379.

24. Detrano R, Guerci AD, Carr JJ, Bild DE, Burke G, Folsom AR, Liu K, Shea S, Szklo M, Bluemke DA, O'Leary DH, Tracy R, Watson K, Wong ND, Kronmal RA. Coronary calcium as a predictor of coronary events in four racial or ethnic groups. *N Engl J Med* 2008;358:1336–1345.

25. Greenland P, LaBree L, Azen SP, Doherty TM, Detrano RC. Coronary artery calcium score combined with Framingham score for risk prediction in asymptomatic individuals. *JAMA* 2004;291:210–215.

26. Jin HY, Weir-McCall JR, Leipsic JA, Son JW, Sellers SL, Shao M, Blanke P, Ahmadi A, Hadamitzky M, Kim YJ, Conte E, Andreini D, Pontone G, Budoff MJ, Gottlieb I, Lee BK, Chun EJ, Cademartiri F, Maffei E, Marques H, de Araujo Goncalves P, Shin S, Choi JH, Virmani R, Samady H, Stone PH, Berman DS, Narula J, Shaw LJ, Bax JJ, Chinnaiyan K, Raff G, Al-Mallah MH, Lin FY, Min JK, Sung JM, Lee SE, Chang HJ. The relationship between coronary calcification and the natural history of coronary artery disease. *JACC Cardiovasc Imaging* 2021;14:233–242.

27. van Rosendael AR, Narula J, Lin FY, van den Hoogen IJ, Gianni U, Al Hussein Alawamlh O, Dunham PC, Pena JM, Lee SE, Andreini D, Cademartiri F, Chinnaiyan K, Chow BJW, Conte E, Cury RC, Feuchtner G, Hadamitzky M, Kim YJ, Leipsic J, Maffei E, Marques H, de Araujo Goncalves P, Plank F, Pontone G, Raff GL, Villines TC, Weirich HG, Al'Aref SJ, Baskaran L, Cho I, Danad I, Han D, Heo R, Lee JH, Rivzi A, Stuijfzand WJ, Gransar H, Lu Y, Sung JM, Park HB, Samady H, Stone PH, Virmani R, Budoff MJ, Berman DS, Chang HJ, Bax JJ, Min JK, Shaw LJ. Association of high-density calcified 1K plaque with risk of acute coronary syndrome. *JAMA Cardiol* 2020;5:282–290.

28. Hoffmann U, Ferencik M, Cury RC, Pena AJ. Coronary CT angiography. *J Nucl Med* 2006;47:797–806.